

On the separability of microscopic optical model potentials and emerging bell-shape Perey-Buck nonlocality

H. F. Arellano¹ and G. Blanchon^{2,3}

¹ Department of Physics - FCFM, University of Chile, Av. Blanco Encalada 2008, Santiago, RM 8370449, Chile

² CEA,DAM,DIF, F-91297 ArpaJon, France

³ Université Paris-Saclay, CEA, Laboratoire Matière en Conditions Extrêmes, Bruyères-le-Châtel, France

Received: date / Revised version: date

Abstract. After nearly sixty years since its introduction, the phenomenological bell-shape Perey-Buck spatial nonlocality in the optical model potential for nucleon-nucleus scattering has remained unaccounted for from a microscopic standpoint. In this article we provide a quantitative account for such nonlocality considering fully nonlocal optical potentials in momentum space. The framework is based on a momentum-space *in-medium* folding model, where infinite nuclear matter g matrices in Brueckner-Hartree-Fock approximation are folded to the target one-body mixed density. The study is based on chiral next-to-next-to-next-to-leading order (N³LO) as well as Argonne v_{18} nucleon-nucleon bare interaction models. Applications focus on $^{40}\text{Ca}(p, p)$ scattering at beam energies in the range 11–200 MeV, resulting in the identification of a separable structure of the momentum-space optical potential of a form we coin as JvH , with a nonlocality form factor as one of its terms. The resulting nonlocality form factor features a bell-shape with nonlocality range β between 0.86 and 0.89 fm, for both proton and neutron beams at energies below 65 MeV. An analytic toy model is introduced to elucidate the underlying mechanism for the nonlocality in the optical model, providing an estimate of its range based on the Fermi motion of the target nucleons and the long-range part of the NN interaction.

PACS. 24.10.Ht Optical models (nuclear reactions) – 03.65.Nk Nonrelativistic theory of scattering – 25.40.Cm, 25.40.Dn Nucleon-induced reactions – 24.10.Cn Many-body theory in nuclear reaction models 28.20.Cz Neutron scattering – 25.40.Cm Proton scattering (nuclear reactions)

1 Introduction

The fermionic nature of nucleons together with many-body correlations constitute two essential aspects for conceiving nonlocality in the coupling between nucleonic probes and nuclei. This feature was early investigated in the late 50s with the introduction of phenomenological optical model potentials with Gaussian nonlocality [1, 2, 3]. Subsequent studies by Perey and Buck in the context of neutron scattering resulted in the construction of an energy-independent nonlocal optical potential [4], with reasonable account of scattering data for aluminum to lead targets at energies in the range 0.4 – 24 MeV. The merit of this construction is that the parameters of the potential were obtained from fits to differential cross section data for $^{208}\text{Pb}(n, n)$ at two energies only, namely 7 and 14.5 MeV. The range of nonlocality of the assumed Gaussian form factor was found to be around 0.85 fm, quantity broadly accepted nowadays but still unaccounted for from a microscopic standpoint.

Some estimates for the range of nonlocality in optical potentials for nucleon scattering have been reported [5, 6, 7], in addition to investigations aimed to identifying its

causes [8, 9]. Additionally, several efforts have been pursued in order to broaden the extent of Perey-Buck-like parametrizations [10, 11, 12]. These works are strongly motivated by the recognized role of nonlocal effects in processes such as (p, d) transfer and capture reactions [13, 14, 15], in addition to dispersive optical models [16, 17, 18].

In this paper we give a quantitative account for the nonlocality in the optical potential for nucleon-nucleus scattering, in addition to its shape. This is achieved after a close scrutiny of the momentum-space structure of microscopic optical potential based on chiral N³LO [19] as well as Argonne v_{18} (AV18) [20] bare nucleon-nucleon (NN) interactions. We show that, to lowest order, the optical potential factorizes in such a way that its nonlocality form factors can be isolated and calculated microscopically. This feature allows parameter-free accounts for the nonlocality shape and range, in addition to information on radial form factors as well as volume integrals.

2 Framework

The nonrelativistic optical potential in momentum space for nucleon elastic scattering off spin-zero nucleus can be cast as [21]

$$\tilde{U}(\mathbf{k}', \mathbf{k}; E) = \tilde{U}_c(\mathbf{k}', \mathbf{k}; E) + i\boldsymbol{\sigma} \cdot \hat{\mathbf{n}} \tilde{U}_{so}(\mathbf{k}', \mathbf{k}; E), \quad (1)$$

with E the center-of-mass (c.m.) energy, $\boldsymbol{\sigma}$ twice the spin of the projectile and $\hat{\mathbf{n}}$ given by $\hat{\mathbf{n}} = \mathbf{k}' \times \mathbf{k} / |\mathbf{k}' \times \mathbf{k}|$. Here \tilde{U}_c and \tilde{U}_{so} denote the central and spin-orbit components of the potential. To evaluate the potential we follow Refs. [22, 23, 24], with an infinite nuclear-matter model to represent the *in-medium* effective NN interaction. Additionally, the use of the Slater approximation for the one-body mixed density yields [22]

$$\begin{aligned} \tilde{U}_\nu(\mathbf{k}', \mathbf{k}; E) = & 4\pi \sum_{\alpha=p,n} \int_0^\infty z^2 dz \rho_\alpha(z) j_0(qz) \\ & \times \int d\mathbf{P} S_z(P) \left\langle \frac{\mathbf{k}' - \mathbf{P}}{2} \left| g_K^{\nu\alpha}(E + \bar{\epsilon}) \right| \frac{\mathbf{k} - \mathbf{P}}{2} \right\rangle_{\mathcal{A}}, \quad (2) \end{aligned}$$

where \mathcal{A} denotes antisymmetrization, ν the nucleonic probe and $\rho_\alpha(z)$ the nuclear density of species α at coordinate z . Additionally, $g^{\nu\alpha}$ is the density-dependent Brueckner-Hartree-Fock (BHF) g matrix, evaluated at the isoscalar density $\rho(z)$, coupling nucleon ν with target nucleon α . In the above S_z is given by

$$S_z(P) = \frac{3}{4\pi k_z^3} \Theta(k_z - P), \quad (3)$$

setting bounds for the off-shell sampling of the g matrix at the radial coordinate z . The local Fermi momentum k_z depends on the isoscalar density $\rho(z)$ at the radial coordinate z through

$$k_z = \left[\frac{3\pi^2 \rho(z)}{2} \right]^{1/3}. \quad (4)$$

Applications of this parameter-free model have been reported in Refs. [22, 25, 24], allowing reasonable descriptions of elastic scattering at nucleon energies from tens of MeV up to about 1 GeV.

The calculations of microscopic optical model potentials we carry out are based on proton and neutron densities from Gogny's D1S Hartree-Fock calculations [26]. Additionally, fully off-shell NN g matrices at fifteen equally spaced Fermi momenta k_F are calculated in momentum space solving the BHF equation for symmetric nuclear matter

$$\hat{g}(\omega) = \hat{v} + \hat{v} \frac{\hat{Q}}{\omega + i\eta - \hat{h}_1 - \hat{h}_2} \hat{g}(\omega), \quad (5)$$

with ω the starting energy, \hat{v} the bare NN interaction, \hat{Q} the Pauli blocking operator suppressing nucleon propagation below the Fermi energy, and $\hat{h}_{1,2}$ nucleons single-particle energies. To solve this integral equation we apply

techniques introduced in Ref. [27]. We stress here that self-consistent g matrix calculations do take into account Cooper eigenvalues in 1S_0 and $^3S_1 - ^3D_1$ [27, 28, 29]. Scattering observables for the resulting nonlocal optical potentials are obtained using SWANLOP package [30] together with SIDES package [31] for double-checks, both treating nonlocalities without approximations.

The consistency of the momentum-space approach adopted here is illustrated in Fig. 1, where we plot the calculated differential cross section for proton elastic scattering off ^{40}Ca at beam energies in the set $\mathcal{E}_6 = \{30.3, 40, 61.4, 80, 135, 200\}$, in MeV units. Solid and dashed curves denote results based on N3LO and AV18 bare interactions, respectively. Nonlocal Pery-Buck-based parametrization by Tian *et al.* [10] (TPM) at 30.3 and 40 MeV are shown with short-dashed curves. The data are from Refs. [32, 33, 34, 35, 36]. We observe that results based on N3LO and AV18 bare potentials yield comparable descriptions of the data, except at 200 MeV where N3LO shows deeper diffraction minima. In the case of TPM parametrization at 40 MeV and below, the calculated ratio-to-Rutherford differential cross sections $\sigma(\theta)/\sigma_R$ appears more diffractive than those from microscopic approaches. Overall, we can state that the parameter-free microscopic approach is able to grasp leading features in the scattering process over a broad energy range.

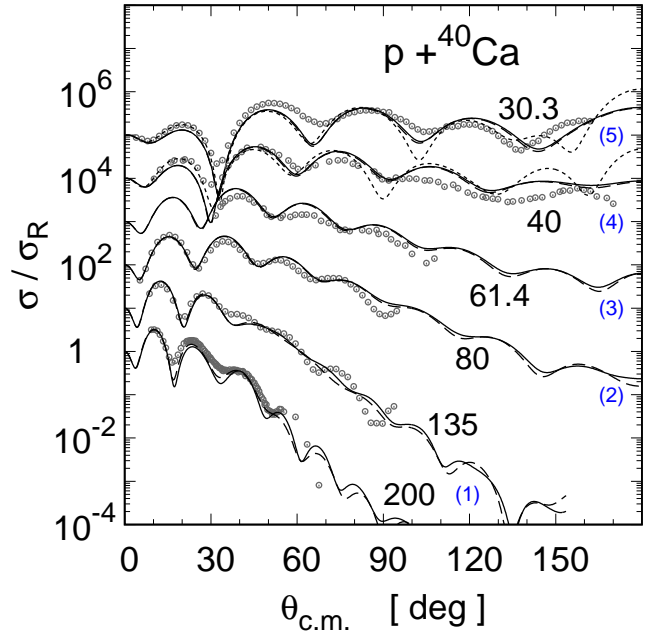


Fig. 1. Ratio-to-Rutherford differential cross sections as function of the c.m. scattering angle for $^{40}\text{Ca}(p, p)$ scattering. Solid and long-dashed curves correspond to momentum-space g -matrix folding potentials using chiral N3LO and AV18 bare interactions, respectively. Short-dashed curves correspond to Pery-Buck model using TPM parametrization. Labels indicate beam energy in MeV units. Numbers in parentheses indicates the power of ten in upshift. The data are from Refs. [32, 33, 34, 35, 36]

2.1 Separability

To examine the momentum-space structure of the potential we find advantageous to re-express it in terms of momentum transfer \mathbf{q} , mean momentum \mathbf{K} and the cosine of their relative angle:

$$\mathbf{q} = \mathbf{k} - \mathbf{k}' ; \quad (6a)$$

$$\mathbf{K} = \frac{1}{2} (\mathbf{k} + \mathbf{k}') ; \quad (6b)$$

$$w = \hat{\mathbf{K}} \cdot \hat{\mathbf{q}} . \quad (6c)$$

Accordingly, we define $\tilde{U}(\mathbf{K}, \mathbf{q}) = \tilde{U}(\mathbf{k}', \mathbf{k}; E)$, so that

$$\tilde{U}(\mathbf{K}, \mathbf{q}) = \tilde{U}_c(K, q; w) + i\sigma \cdot (\mathbf{K} \times \mathbf{q}) \tilde{U}_{so}(K, q; w) , \quad (7)$$

leaving the dependence on E implicit. In Fig. 2 we show a surface plot of $\tilde{U}_c(K, q, w)$ in the Kq plane for the case of $\text{Ca}(p, p)$ scattering at 40 MeV. For this plot we have chosen $\mathbf{K} \perp \mathbf{q}$, namely $w = 0$. The real part of the potential is shown with colored surface, whereas its imaginary part is shown with a black mesh. We observe that the potential exhibits a smooth behavior in both, K and q momenta, decreasing for increasing momenta.

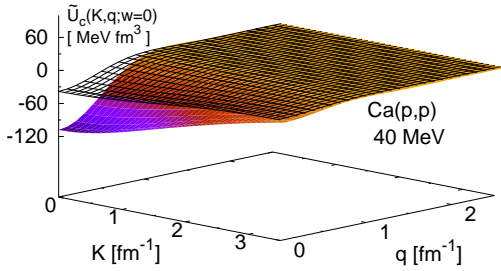


Fig. 2. Surface plots in the Kq plane of the central optical potential $\tilde{U}_c(K, q; w = 0)$, for $^{40}\text{Ca}(p, p)$ scattering at 40 MeV. The colored surface represents its real part and the black mesh its imaginary component. Results from momentum-space g -matrix folding potentials based on AV18 bare NN potential.

We have investigated the w -dependence of \tilde{U}_c and \tilde{U}_{so} for microscopic potentials at all energies in \mathcal{E}_6 , including lower energies, finding it very weak. To illustrate the weak angular dependence we have calculated the normalized difference

$$\delta\tilde{U}_c(K, q) = \frac{1}{\tilde{U}_c(0,0;0)} \left[\tilde{U}_c(K, q; w_1) - \tilde{U}_c(K, q; w_2) \right] , \quad (8)$$

considering $w_1 = 0$, and $w_2 = 1$. Under this definition $\delta\tilde{U}_c$ becomes dimensionless and equal to unity for $K = q = 0$. We have examined $\delta\tilde{U}_c$ separately for the coupling of the projectile (protons) to target protons (pp) and target neutrons (pn). In Fig. 3 we show surface plots of $\delta\tilde{U}_c(K, q)$ as a function of K and q , at beam energies of 21 (a,b) and 200 MeV (c,d). The real parts are shown with colored surfaces whereas their imaginary parts are shown with orange meshes. As observed, the difference is negligible for

$K \lesssim 1.5 \text{ fm}^{-1}$, exhibiting some structure below $\sim 1\%$ at q below 1 fm^{-1} . Similar features are observed for the spin-orbit term.

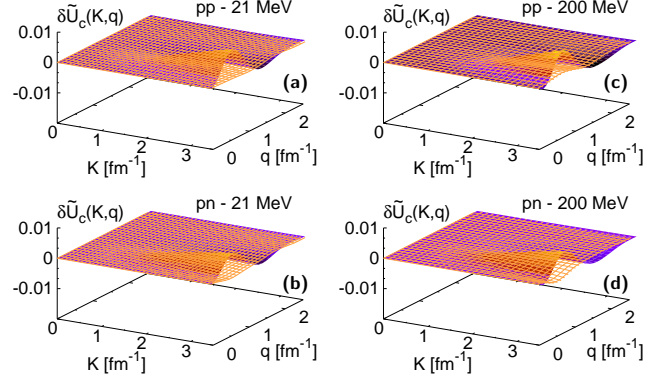


Fig. 3. Surface plots in the Kq plane for the real and imaginary components of $\delta\tilde{U}_c(K, q)$, for $^{40}\text{Ca}(p, p)$ scattering at 21(a,b) and 200 MeV (c,d). Results from momentum-space g -matrix folding potentials based on AV18 bare NN potential.

The above results justify to ignore (to lowest order) the w -dependence in the optical potential, assigning

$$\tilde{U}_c(K, q; w) \rightarrow \tilde{U}_c(K, q) , \quad (9a)$$

$$|\mathbf{K} \times \mathbf{q}| \tilde{U}_{so}(K, q; w) \rightarrow Kq\sqrt{1-w^2} \tilde{U}_{so}(K, q) . \quad (9b)$$

As a way to remove the w dependence we use $w = 0$, choice that ensures symmetric relative momenta, i.e. $k = k'$.

To disentangle the structure of $\tilde{U}_c(K, q)$ and $\tilde{U}_{so}(K, q)$ in the Kq plane, let us define $W_c = \tilde{U}_c(0, 0)$ and

$$\tilde{V}_c(K, q) = \frac{\tilde{U}_c(K, q)}{\tilde{U}_c(K, 0)} ; \quad (10a)$$

$$\tilde{H}_c(K) = \frac{\tilde{U}_c(K, 0)}{\tilde{U}_c(0, 0)} ; \quad (10b)$$

so that

$$\tilde{U}_c(K, q) = W_c \tilde{V}_c(K, q) \tilde{H}_c(K) . \quad (11)$$

An analogous construction is applied to the spin-orbit term, resulting in

$$\tilde{U}_{so}(K, q) = W_{so} \tilde{V}_{so}(K, q) \tilde{H}_{so}(K) . \quad (12)$$

Note that $\tilde{V}_c(K, q)$, $\tilde{H}_c(K)$, $\tilde{V}_{so}(K, q)$ and $\tilde{H}_{so}(K)$ are dimensionless quantities satisfying $\tilde{V}_c(K, 0) = \tilde{V}_{so}(K, 0) = 1$, and $\tilde{H}_c(0) = \tilde{H}_{so}(0) = 1$. It is also worth stating that, in connection to Perey-Buck notation [4], (K, q) momenta are the conjugate variables of their (s, R) coordinates.

We now proceed to examine separately the three terms on the right-hand-side of Eqs. (11) and (12). We have investigated the momentum dependence of $\tilde{V}_c(K, q)$ and $\tilde{V}_{so}(K, q)$ at all energies in \mathcal{E}_6 . We found that their dependence on K is remarkably weak. This feature is illustrated in Fig. 4, where we show surface plots of $\text{Re } \tilde{V}_c(K, q)$ and

Im $\tilde{V}_c(K, q)$, in the Kq plane. The energies considered here are 21 (a), 40 (b), 80 (c) and 200 (d) MeV. Note the close resemblance of all four surfaces, despite the broad energy range they span, exhibiting small imaginary parts in all cases. These features are also observed in the spin-orbit term \tilde{V}_{so} .

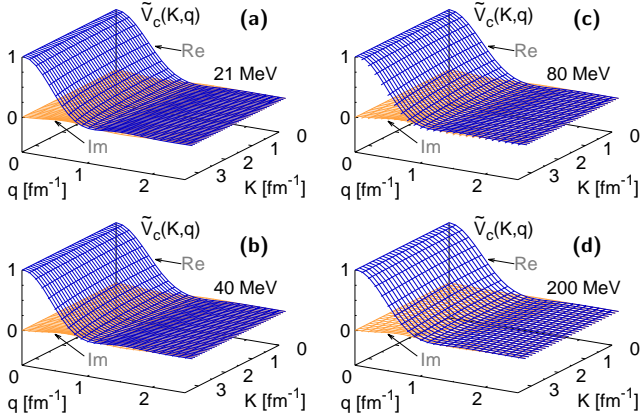


Fig. 4. Surface plots in the Kq plane for the real and imaginary components of $\tilde{V}_c(K, q)$, for $^{40}\text{Ca}(p, p)$ scattering at 21(a), 40(b), 80(c) and 200(d) MeV. Results from momentum-space g -matrix folding potentials based on AV18 bare NN potential.

The potential U_{pA} for proton-nucleus scattering can be decomposed as

$$U_{pA} = U_{pp} + U_{pn}, \quad (13)$$

where the subscripts pp and pn denote coupling of the incident proton with target protons and neutrons, respectively. To each of these three terms we investigate the factorization (11), labeling them as p - A , p - p and p - n , respectively. Considering the weak dependence of $\tilde{V}_c(K, q)$ and $\tilde{V}_{so}(K, q)$ on K , in Fig. 5 we plot the radial form factors $\tilde{v}_c(q) \equiv \tilde{V}_c(0, q)$, and $\tilde{v}_{so}(q) \equiv \tilde{V}_{so}(0, q)$, as functions of q for all energies in \mathcal{E}_6 . Upper (Lower) panels correspond to potentials based on N3LO (AV18) bare NN interactions. Central (c) and spin-orbit (so) components are plotted with black and red curves, respectively. Panels (a,d) correspond to p - A coupling; (b,e) to p - p coupling; and (c,f) to p - n coupling. The shaded areas denote Fourier transforms of the isoscalar, proton and neutron densities for ^{40}Ca used in these calculations. The similarity of all six curves, particularly in their real parts, point to a weak energy dependence of both central and spin-orbit terms. The imaginary component shows more differences, but remaining weaker relative to their real parts. When comparing N3LO- and AV18-based potentials, differences are noticed in the real spin-orbit (red curves). Such differences suggest shorter range in $\text{Re } \tilde{v}_{so}$ for the AV18- relative to N3LO-based interactions.

Let us now focus on $\tilde{H}_c(K)$ and $\tilde{H}_{so}(K)$, both directly related to the nonlocality of the potential. In the Perey-Buck model the nonlocal form factor in coordinate space

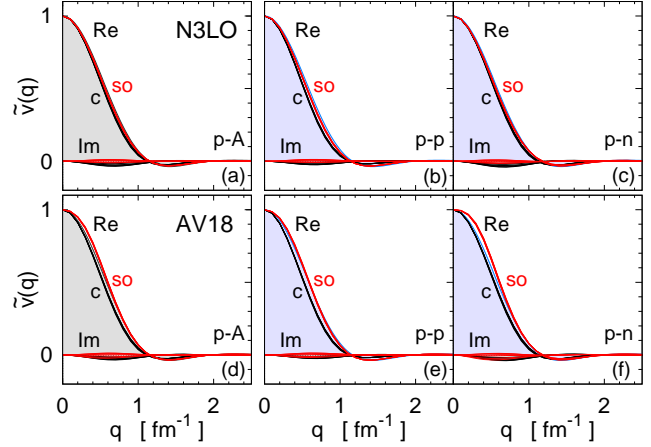


Fig. 5. Radial form factor $\tilde{v}_c(q)$ for $^{40}\text{Ca}(p, p)$ scattering based on N3LO and AV18 bare NN potentials. Panels (a,d), (b,e) and (c,f) show results for p - A , p - p and p - n couplings, respectively.

is defined as

$$H_{PB}(s) = \frac{1}{\pi^{3/2}\beta^3} e^{-s^2/\beta^2}, \quad (14)$$

with s the difference between prior and post relative coordinates and β the range of nonlocality. In momentum space,

$$\tilde{H}_{PB}(K) = e^{-\beta^2 K^2/4}. \quad (15)$$

As done for $\tilde{v}(q)$ in Fig. 5, we analyze separately the p - A , p - p and p - n terms. In Fig. 6 we plot $\tilde{H}(K)$ calculated from momentum-space folding potentials at all energies in \mathcal{E}_6 . Panels and labels are the same as in Fig. 5. Solid black and blue curves correspond to proton beam energy of 30.3 and 200 MeV, respectively. Dashed red curves represent results for 61.4 MeV. The shaded areas represent Perey-Buck form factor with $\beta = 0.84$ fm.

From Fig. 6 we observe that $\text{Re } \tilde{H}_c(K)$ for N3LO- and AV18-based potentials exhibit similar patterns at all energies, all of them featuring a bell shape. In particular, both p - A and p - n appear quite similar to Perey-Buck's form factor \tilde{H}_{PB} , in contrast to p - p where weaker curvatures takes place at the origin. This feature implies that for p - p coupling, the associated nonlocality range is smaller than that for \tilde{H}_{PB} . With regard to the spin-orbit form factor, we notice that $\text{Re } \tilde{H}_{so}(K)$ is quite disperse for p - A and p - n , particularly above 61.4 MeV (dashed red curves). Furthermore, curvatures of \tilde{H}_{so} are consistently smaller than those for \tilde{H}_c , pointing to smaller range of nonlocality relative to the central part. We also note that $\text{Re } \tilde{H}_{so}(K)$ follow a similar trend, although their curvatures near $K=0$ appear weaker.

In Table 1 we tabulate the calculated β as function of the proton energy from Gaussian fits of $\text{Re } \tilde{H}(K) = \exp(-\beta^2 K^2/4)$, over the range $0 \leq K \leq 1$ fm $^{-1}$. To illustrate the trend of these results at lower energies we include 11.42 and 21 MeV. We observe that β_{pA} in the central channel varies 3% at most at energies below 80 MeV,

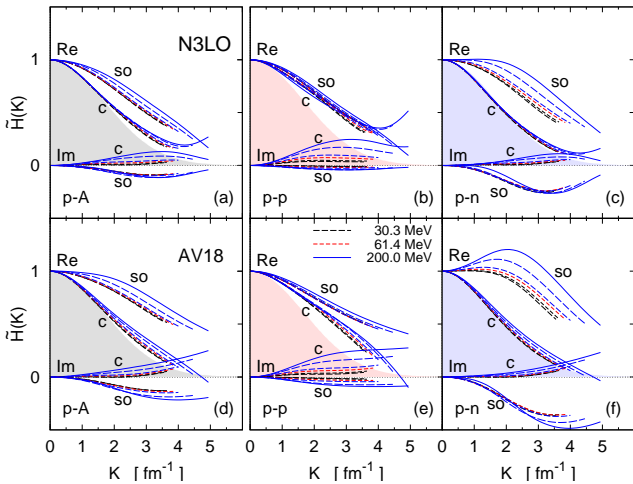


Fig. 6. Bell-shape nonlocality form factor $\tilde{H}(K)$ from momentum-space g -matrix folding potentials in energy set \mathcal{E}_6 . Results for central (c) and spin-orbit (so), based on N3LO and AV18 bare NN potentials. Panels (a,d), (b,e) and (c,f) show form factors for p - A , p - p and p - n couplings, respectively. The shaded areas denote Perey-Buck nonlocality form factor with $\beta = 0.84$ fm.

for both N3LO- and AV18-based microscopic potentials. We also note that $\beta_{pn} - \beta_{pp} \approx 0.22$ fm, in all cases below 100 MeV, indicating that the coupling of protons to target neutrons is slightly more nonlocal than the coupling to protons. A similar trend is observed in calculations made for neutron scattering. The above values for the range of nonlocality are consistent with PB reported value $\beta_n = 0.85$ fm, and TPM values $\beta_n = 0.90$ fm, and $\beta_p = 0.88$ fm.

In the spin-orbit sector of Table 1, entries with dashes correspond to cases with positive curvature for \tilde{H} at the origin. This feature occurs in the p - n coupling using AV18 bare potential. This peculiarity gets manifested in β_{pA} , resulting in a more local p - A coupling for AV18- relative to N3LO-based potential. What is remarkable from these results is that the spin-orbit term of the optical potential also exhibits a bell-shape nonlocality, although such nonlocality appears smaller than in the central part by about 0.3–0.4 fm. This is in contrast with Perey-Buck model, where the spin-orbit term is local. This result is interesting in the context of phenomenological constructions of nonlocal potentials, suggesting a prescription to include nonlocality in the spin-orbit term.

We have also investigated the range of nonlocality β in the case of neutron scattering. Results are summarized in Table 2, for neutron energies between 10 and 65 MeV, following the same convention as in Table 1. As observed, β_{nA} is very similar to β_{pA} for both, central and spin-orbit components.

In Fig. 7 we plot β as a function of the energy for proton (black curves) and neutron (red curves) scattering off ^{40}Ca , to be called β_p and β_n , respectively. Solid and dashed curves denote results based on N3LO and AV18 interactions, respectively. We include results for the cen-

tral (c) and spin-orbit (so). As observed, for a given NN interaction, β_p and β_n in the central part are quite similar to each other, with differences below $\sim 1\%$ when comparing N3LO with AV18. In the case of the spin-orbit term, under a given bare interaction the differences between β_p and β_n are below 1%. However, the nonlocality obtained from N3LO becomes larger by about 1 fm relative to that based on AV18. Overall, Fig. 7 shows weak energy dependence of β in all cases.

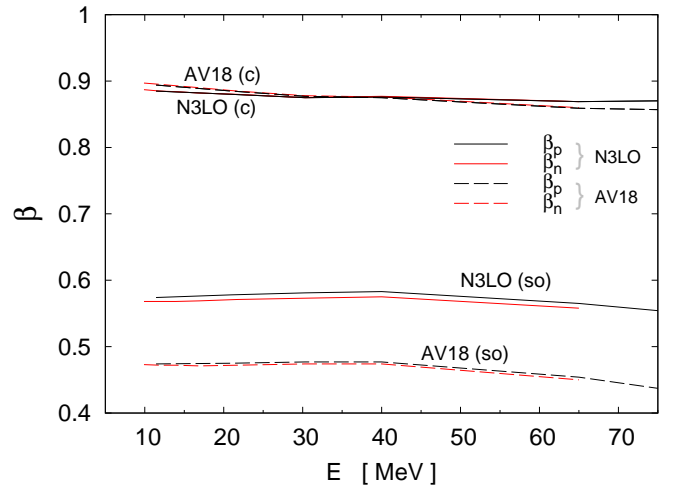


Fig. 7. Energy dependence of the range of nonlocality for proton (β_p) and neutron (β_n) scattering off ^{40}Ca . Results for the central (c) and spin-orbit (so) parts of the potential, based on chiral N3LO (solid curves) and AV18 (dashed curves) bare interactions.

Another term in factorization (11) is W , corresponding to the potential for zero momenta. This strength is directly related to the volume integral J of the potential [30], namely

$$W = \frac{J}{(2\pi)^3}. \quad (16)$$

In Fig. 8 we show the central (W_c) and spin-orbit (W_{so}) strength as function of the beam energy, where solid (dashed) curves denote results based on N3LO (AV18) bare interaction. We observe that the p - n strength is stronger than its p - p counterpart in all channels. It also becomes evident that both p - n and p - p parts are nearly energy independent, except for $\text{Re } W_c$ in the p - n coupling which changes by 12% in the range 11–40 MeV. The spin-orbit strengths W_{so} , in turn, are quite small relative to the central part, nearly vanishing for $\text{Im } W_{so}$ in p - n coupling.

2.2 The JvH factorization

In order to assess the ability of the three factors in Eq. (11) to retain the original description of σ/σ_R , we introduce the

		N3LO			AV18		
Energy (MeV)		β_{pA} (fm)	β_{pp} (fm)	β_{pn} (fm)	β_{pA} (fm)	β_{pp} (fm)	β_{pn} (fm)
Central	11.42	0.89	0.72	0.94	0.89	0.73	0.95
	21.0	0.88	0.72	0.94	0.89	0.72	0.94
	30.3	0.88	0.71	0.93	0.88	0.71	0.94
	40.0	0.88	0.71	0.93	0.88	0.71	0.93
	61.4	0.87	0.72	0.93	0.86	0.70	0.92
	80.0	0.87	0.72	0.93	0.86	0.71	0.92
	135.0	0.87	0.75	0.92	0.83	0.71	0.89
	200.0	0.86	0.78	0.90	0.80	0.72	0.85
Spin-orbit	11.42	0.57	0.61	0.51	0.47	0.58	0.03
	21.0	0.58	0.61	0.50	0.46	0.59	—
	30.3	0.58	0.62	0.49	0.48	0.59	—
	40.0	0.58	0.63	0.48	0.48	0.60	—
	61.4	0.57	0.63	0.43	0.46	0.60	—
	80.0	0.55	0.62	0.37	0.37	0.59	—
	135.0	0.48	0.59	0.13	0.32	0.56	—
	200.0	0.44	0.56	—	0.22	0.51	—

Table 1. Central and spin-orbit nonlocality β_p for $p+^{40}\text{Ca}$ scattering as functions of the energy from momentum-space folding potentials based on chiral N3LO and AV18 bare interactions.

		N3LO			AV18		
Energy (MeV)		β_{nA} (fm)	β_{np} (fm)	β_{nn} (fm)	β_{nA} (fm)	β_{np} (fm)	β_{nn} (fm)
Central	11.9	0.89	0.94	0.72	0.90	0.95	0.73
	21.7	0.88	0.94	0.72	0.89	0.94	0.72
	30.3	0.88	0.93	0.71	0.88	0.94	0.71
	40.0	0.88	0.94	0.71	0.88	0.94	0.71
	65.0	0.88	0.93	0.71	0.86	0.92	0.70
Spin-orbit	11.9	0.57	0.50	0.60	0.47	0.03	0.58
	21.7	0.57	0.50	0.60	0.47	—	0.58
	30.3	0.57	0.49	0.61	0.47	—	0.59
	40.0	0.58	0.48	0.62	0.47	—	0.60
	65.0	0.56	0.42	0.62	0.45	—	0.60

Table 2. Central and spin-orbit nonlocality β_n for $n+^{40}\text{Ca}$ scattering as functions of the energy from momentum-space folding potentials based on chiral N3LO and AV18 bare interactions.

separable representation

$$\tilde{U}(K, q) = W_c \tilde{v}_c(q) \tilde{H}_c(K) + i \boldsymbol{\sigma} \cdot (\mathbf{K} \times \mathbf{q}) W_{so} \tilde{v}_{so}(q) \tilde{H}_{so}(K). \quad (17)$$

We will refer to this decomposition as JvH factorization, being comprised by the strength $W = J/(2\pi)^3$, the normalized radial form factor \tilde{v} and the normalized nonlocality form factor \tilde{H} . Implicit in this construction is that the w -dependence of \tilde{U}_c and \tilde{U}_{so} in Eq. (7), and K -dependence of $\tilde{V}(K, q)$, are weak.

In Fig. 9 we show results for the ratio-to-Rutherford differential cross sections for $^{40}\text{Ca}(p, p)$ scattering from momentum-space folding potentials (gray shaded) and corresponding JvH form (red shaded). Solid and short-dashed curves denote N3LO- and AV18-based results, respectively. Results are shown as functions of the c.m. scattering angle $\theta_{c.m.}$. In these plots we include applications at 11.4 and 21 MeV. As observed in panel (a) at energies up

to 40 MeV, close agreement takes place between the original potential and its JvH representation. This is noted by comparing gray- vs red-shaded areas, although discrepancies appear at 40 MeV above 120 deg. In panel (b) for the higher energies, however, differences become evident at angles above the second minimum, roughly around 25 deg.

An important element for the separability of the optical potential is its weak dependence on $w = \hat{K} \cdot \hat{q}$. This is in line with a recent study of Burrows *et al.* [37] on features of the nonlocal one-body density $[\rho(q, \mathcal{K})$ in their notation]. The authors also find that the largest contribution to the nonlocal density comes from s waves, with an associated nonlocality of about 2 fm. In actual calculations of the optical potential, these features in the one-body mixed density need to be convoluted with the effective interaction. Its implications on the nonlocality of the optical potential is illustrated in the following section with the introduction of a toy model.

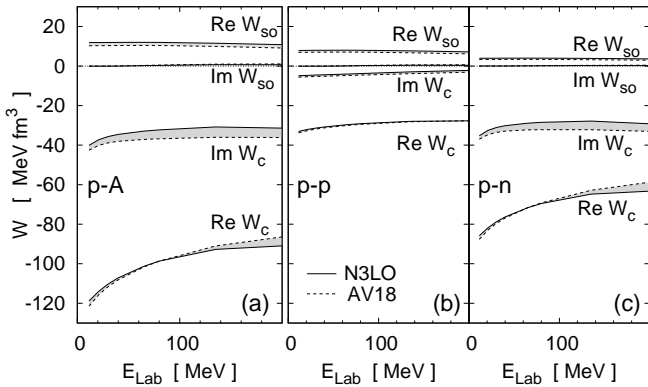


Fig. 8. Energy dependence of the real and imaginary components of volume strengths W_c and W_{so} . Results for $^{40}\text{Ca}(p,p)$ scattering considering N3LO (solid curves) and AV18 (dashed curves) bare potentials. Panels (a), (b) and (c) show results for p -A, p - p and p - n couplings, respectively.

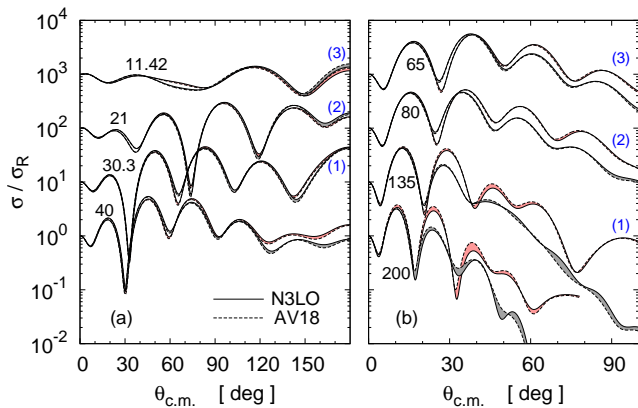


Fig. 9. Ratio-to-Rutherford differential cross sections as functions of $\theta_{c.m.}$ for $^{40}\text{Ca}(p,p)$ scattering from momentum-space folding potentials (gray shaded areas) and its JvH form (red shaded areas). Solid (short-dashed) curves denote results using N3LO (AV18) interactions. Labels indicate beam energy in MeV units. Numbers in parentheses denote power of ten of upshift.

2.3 Toy model

An interesting outcome from this study is that the microscopic momentum-space optical model potential summarized by Eq. (2) accounts consistently for the range of nonlocality in PB and TPM models obtained phenomenologically. We now devise a toy model aiming to understand the role of physical elements responsible of the range of nonlocality in the optical model. The parameter-free approach used here involves the folding of an antisymmetrized Fermi-motion-averaged effective interaction. With these elements in mind let us consider a uniform nuclear density over a sphere of radius R with bulk Fermi momentum $k_z \rightarrow \bar{k}_F$.

In the Slater approximation the one-body mixed density, $\rho(\mathbf{r}_2, \mathbf{r}_1) = \sum_\nu \phi_\nu^\dagger(\mathbf{r}_2)\phi_\nu(\mathbf{r}_1)$, can be approximated

as [38]

$$\rho(\mathbf{r}_2, \mathbf{r}_1) \approx \rho(z)\hat{j}_1(k_F s), \quad (18)$$

with $z = \frac{1}{2}|\mathbf{r}_1 + \mathbf{r}_2|$, $s = |\mathbf{r}_1 - \mathbf{r}_2|$, and $k_F = (3\pi^2\rho)^{1/3}$, being ρ the proton or neutron density. Additionally, $\hat{j}_1(x) \equiv 3j_1(x)/x$. In the case of a uniform sphere the mixed density in momentum space gets expressed as [39]

$$\tilde{\rho}(\mathbf{q}; P) = \tilde{\rho}(\mathbf{q}) \times \frac{3}{4\pi\bar{k}_F^3} \Theta(\bar{k}_F - P), \quad (19)$$

with \mathbf{q} and \mathbf{P} the conjugate coordinates of \mathbf{z} and \mathbf{s} , respectively. The nonlocality of the mixed density is driven by its dependence on P (denoted as \mathcal{K} in Ref. [37]), limited by a bulk Fermi momentum \bar{k}_F . As we shall see next, this feature becomes relevant for the resulting nonlocality of the potential.

Let us now consider the Yukawa-type effective interaction

$$v_{\text{eff}}(r) = g_0 Y(\mu r), \quad (20)$$

with $Y(x) = e^{-x}/x$, where g_0 and μ stand for strength and meson mass, respectively. In momentum representation,

$$\tilde{v}_{\text{eff}}(\mathbf{p}', \mathbf{p}) = \frac{1}{2\pi^2\mu} \frac{g_0}{(\mathbf{p}' - \mathbf{p})^2 + \mu^2}. \quad (21)$$

Replacing this term in Eq. (2), including its $\tilde{v}_{\text{eff}}(\mathbf{p}', -\mathbf{p})$ exchange term, we obtain for nucleon species α

$$U_\alpha(K, 0) = \frac{N_\alpha}{2\pi^2} \frac{3g_0}{4\pi\bar{k}_F^3\mu} \int d\mathbf{P} \times \Theta(\bar{k}_F - P) \left[\frac{1}{\mu^2} \pm \frac{1}{(\mathbf{K} - \mathbf{P})^2 + \mu^2} \right], \quad (22)$$

with N_α the number of protons or neutrons. The \pm signs depend on the spin-isospin parity of the channel involved, consistent with Pauli exclusion principle. Considering singlet-even NN states as leading contributions to \tilde{U} , we select the plus sign. The above integral can then be performed analytically, providing closed expressions for $\tilde{H}(K)$. Additionally, a Taylor expansion of U_α in powers of K^2 allows to extract β as function of the bulk Fermi momentum \bar{k}_F and mass μ . Details are given in A. We use these analytic results to the case of the Michigan-three-Yukawa (M3Y) interaction [40], where

$$v_{\text{eff}}(r) = \sum_{i=1}^3 g_i Y(\mu_i r), \quad (23)$$

with $\mu_3 = m_\pi$, the pion mass. This third term accounts for the long range of the interaction, being dominant in the resulting range of nonlocality.

In Fig. 10 we plot the nonlocality form factor $\tilde{H}(K)$ as function of K considering the M3Y interaction (solid curves). Dashed and dotted curves represent Perey-Buck nonlocality form factor $\tilde{H}_{PB}(K)$ with $\beta = 0.8$ and 0.9 fm, respectively. We observe that, despite the simplicity of the toy model, it is reasonably consistent with PB for $K \lesssim 1 \text{ fm}^{-1}$. The inset of Fig. 10 shows the resulting β

as function of the bulk Fermi momentum \bar{k}_F . To emulate changes in the long range part of the interaction we include results with μ_3 increased (dashed) and decreased (dotted) by 10%. The shaded strip denotes $0.8 \leq \beta \leq 0.9 \text{ fm}^{-1}$, with the box denoting $1.1 \leq \bar{k}_F \leq 1.2 \text{ fm}^{-1}$. These bulk Fermi momenta are similar to those obtained from density-weighted local Fermi momentum k_z in ^{40}Ca and ^{208}Pb , respectively. It is interesting to observe, from this simple model, that the range of nonlocality is mainly driven by the range of the effective interaction together with the bulk Fermi momentum of the nucleus.

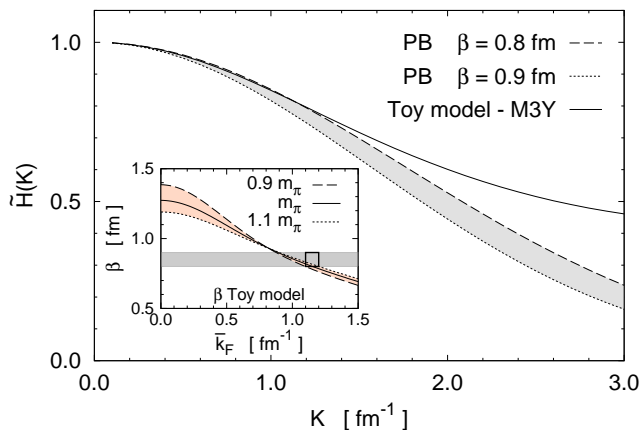


Fig. 10. Nonlocality form factor from toy model (solid curve). Dashed and dotted curves correspond to \tilde{H}_{PB} with $\beta = 0.8$ and 0.9 fm , respectively. Inset shows β as function of the bulk Fermi momentum \bar{k}_F in the toy model.

3 Conclusions

Based on a momentum-space g -matrix approach for the optical model potential, we present the first quantitative account for Perey-Buck range of nonlocality together with its implied form factor. The nonlocality form factor exhibits a bell-shape, thought not strictly Gaussian. These findings result from an analysis of the structure of microscopic potentials based on chiral N3LO as well as AV18 NN bare interaction models. We find that, when the potential is expressed as a function of momenta \mathbf{q} and \mathbf{K} , its lowest order term in angular expansion leads to the so called JvH separable structure for the central and spin-orbit parts of the potential. In this factorization, J corresponds to the volume integral whereas \tilde{v} and \tilde{H} represent normalized radial and nonlocality form factors, respectively. We find that, while the radial form factor is usually represented as Woods-Saxon form factor in phenomenological studies, the nonlocality form factor exhibits close resemblance to that of Perey and Buck [4].

At nucleon energies below 65 MeV the range of nonlocality β for the central potential ends up in the range $0.86 - 0.89 \text{ fm}$, in agreement with phenomenological studies. In the case of the spin-orbit component of the potential the range of nonlocality is in the range $0.46 - 0.58 \text{ fm}$,

smaller than its central part. Beyond its ability to account for near-Gaussian nonlocality form factors and the accepted range of nonlocality β , the JvH factorization offers a novel and well defined link between theory and phenomenology. The possibility to separate the coupling of the projectile with target protons and neutrons offers an interesting route for exploring nonlocality for isospin-asymmetric targets. Thus, the JvH factorization could be useful for assertive microscopic guidance to enhance phenomenological representations of nonlocality in NA scattering phenomena.

The microscopic optical model applied in this study, summarized by Eq. (2), has the advantage of requiring only radial densities. However, the more general model discussed in Refs. [23,24] allows for an explicit treatment of the nonlocal one-body mixed density. Therefore, it would be of interest to assess the implications of the full one-body mixed densities on the nonlocality form factor of the optical potential.

A Integrals for the toy model

To evaluate explicitly Eq. (22) for the toy model using M3Y we pay attention to the direct and exchange terms

$$f_d(\bar{k}_F, \mu) = \frac{3}{4\pi\bar{k}_F^3\mu} \int d\mathbf{P} \Theta(\bar{k}_F - P) \frac{1}{\mu^2} \quad (\text{A.1})$$

$$f_x(K, \bar{k}_F, \mu) = \frac{3}{4\pi\bar{k}_F^3\mu} \int d\mathbf{P} \frac{\Theta(\bar{k}_F - P)}{(K - P)^2 + \mu^2}. \quad (\text{A.2})$$

For the direct term f_d we obtain

$$f_d = \frac{1}{\mu^3}, \quad (\text{A.3})$$

whereas for the exchange term f_x we get

$$f_x = \frac{3}{2\bar{k}_F^3\mu} \int_0^{\bar{k}_F} P^2 dP \int_{-1}^1 \frac{du}{K^2 + P^2 - 2KPu + \mu^2}. \quad (\text{A.4})$$

After angular integration we obtain

$$f_x = \frac{3}{4k\bar{k}_F^3} \int_0^{\bar{k}_F/\mu} x \ln \left[\frac{(k+x)^2 + 1}{(k-x)^2 + 1} \right] dx, \quad (\text{A.5})$$

where we have defined

$$k = \frac{K}{\mu}. \quad (\text{A.6})$$

The calculation of f_x in Eq. (A.5) can be performed analytically. If we denote

$$y = \frac{\bar{k}_F}{\mu}, \quad (\text{A.7})$$

after some algebraic work we obtain

$$f_x = \frac{3}{2y^3\mu^3} \left\{ y - \text{Arctan} \left[\frac{2y}{1+k^2-y^2} \right] + \frac{1+k^2-y^2}{4k} \ln \left[\frac{1+(k+y)^2}{1+(k-y)^2} \right] \right\}, \quad (\text{A.8})$$

where the identity $\text{Arctanh}(z) = \frac{1}{2} \ln[(1+z)/(1-z)]$, was used.

Since leading contributions to the optical potential take place for singlet-even NN channels, we select the plus sign for the exchange term in Eq. (22). Thus,

$$f_d + f_x = \frac{1}{\mu^3} \left(1 + \frac{3}{2y^3} \left\{ y - \text{Arctan} \left[\frac{2y}{1+k^2-y^2} \right] + \frac{1+y^2-k^2}{4k} \ln \left[\frac{1+(k+y)^2}{1+(k-y)^2} \right] \right\} \right) \quad (\text{A.9})$$

$$\equiv \frac{1}{\mu^3} F(y, k). \quad (\text{A.10})$$

To infer the low- K behavior we expand $F(\mu, y, k)$ to second order in k ,

$$F(y, k) = F_0(y) - F_2(y)k^2 + \mathcal{O}(k^4), \quad (\text{A.11})$$

where

$$F_0(y) = 1 + \frac{3}{y^2} - \frac{3}{y^3} \text{Arctan}(y); \quad (\text{A.12a})$$

$$F_2(y) = \frac{1}{(1+y^2)^2}. \quad (\text{A.12b})$$

In the context of the M3Y interaction, the results in Eqs. (A.9), (A.12a) and (A.12b) have been used to obtain U in Eq. (22), together with the implied nonlocality.

References

- W. E. Frahn, On the nucleon-nucleus interaction, *Il Nuovo Cimento* (1956) 313–322 doi:10.1007/BF02745452. URL <https://doi.org/10.1007/BF02745452>
- W. E. Frahn, R. H. Lemmer, Effective nuclear potentials, *Il Nuovo Cimento* (1957) 523 doi:10.1007/BF02855261. URL <https://doi.org/10.1007/BF02855261>
- P. J. Wyatt, J. G. Wills, A. E. S. Green, Nonlocal optical model for nucleon-nuclear interactions, *Phys. Rev.* 119 (1960) 1031–1042. doi:10.1103/PhysRev.119.1031. URL <https://link.aps.org/doi/10.1103/PhysRev.119.1031>
- F. Perey, B. Buck, A non-local potential model for the scattering of neutrons by nuclei, *Nuclear Physics* 32 (1962) 353–380. doi:10.1016/0029-5582(62)90345-0. URL <https://www.sciencedirect.com/science/article/pii/0029558262903450>
- G. Ripka, The non-locality of the optical potential, *Nuclear Physics* 42 (1963) 75–85. doi:https://doi.org/10.1016/0029-5582(63)90715-6. URL <https://www.sciencedirect.com/science/article/pii/0029558263907156>
- M. Giannini, G. Ricco, An energy-independent non-local potential model for bound and scattering states, *Annals of Physics* 102 (2) (1976) 458–492. doi:https://doi.org/10.1016/0003-4916(76)90176-7. URL <https://www.sciencedirect.com/science/article/pii/0003491676901767>
- J. P. Jeukenne, A. Lejeune, C. Mahaux, Many-body theory of nuclear matter, *Phys. Rep.* 25 (2) (1976) 83. doi:10.1016/0370-1573(76)90017-X. URL [http://dx.doi.org/10.1016/0370-1573\(76\)90017-X](http://dx.doi.org/10.1016/0370-1573(76)90017-X)
- G. H. Rawitscher, Interpretation of the Perey-Buck nonlocality in terms of the relativistic optical model formalism, *Phys. Rev. C* 31 (1985) 1173–1178. doi:10.1103/PhysRevC.31.1173. URL <https://link.aps.org/doi/10.1103/PhysRevC.31.1173>
- P. Fraser, K. Amos, S. Karataglidis, L. Canton, G. Pisent, J. P. Svenne, Two causes of nonlocalities in nucleon-nucleus potentials and their effects in nucleon-nucleus scattering, *Eur. Phys. Journal A* (2008) 69 – 80 doi:10.1140/epja/i2007-10524-1. URL <https://doi.org/10.1140/epja/i2007-10524-1>
- Y. Tian, D.-Y. Pang, Z.-Y. Ma, Systematic nonlocal optical model potential for nucleons, *International Journal of Modern Physics E* 24 (01) (2015) 1550006. doi:10.1142/S0218301315500068. URL <https://www.worldscientific.com/doi/abs/10.1142/S0218301315500068>
- A. E. Lovell, P.-L. Bacq, P. Capel, F. M. Nunes, L. J. Titus, Energy dependence of nonlocal optical potentials, *Phys. Rev. C* 96 (2017) 051601(R). doi:10.1103/PhysRevC.96.051601. URL <https://link.aps.org/doi/10.1103/PhysRevC.96.051601>
- M. I. Jaghoub, A. E. Lovell, F. M. Nunes, Exploration of the energy dependence of proton nonlocal optical potentials, *Phys. Rev. C* 98 (2018) 024609. doi:10.1103/PhysRevC.98.024609. URL <https://link.aps.org/doi/10.1103/PhysRevC.98.024609>
- A. Ross, L. J. Titus, F. M. Nunes, M. H. Mahzoon, W. H. Dickhoff, R. J. Charity, Effects of nonlocal potentials on (p, d) transfer reactions, *Phys. Rev. C* 92 (2015) 044607. doi:10.1103/PhysRevC.92.044607. URL <https://link.aps.org/doi/10.1103/PhysRevC.92.044607>
- G. W. Bailey, N. K. Timofeyuk, J. A. Tostevin, Nonlocal nucleon-nucleus interactions in (d, p) reactions: Role of the deuteron D state, *Phys. Rev. C* 95 (2017) 024603. doi:10.1103/PhysRevC.95.024603. URL <https://link.aps.org/doi/10.1103/PhysRevC.95.024603>
- Y. Tian, D. Y. Pang, Z.-y. Ma, Effects of nonlocality of nuclear potentials on direct capture reactions, *Phys. Rev. C* 97 (2018) 064615. doi:10.1103/PhysRevC.97.064615. URL <https://link.aps.org/doi/10.1103/PhysRevC.97.064615>
- W. H. Dickhoff, D. Van Neck, S. J. Waldecker, R. J. Charity, L. G. Sobotka, Nonlocal extension of the dispersive optical model to describe data below the Fermi energy, *Phys. Rev. C* 82 (2010) 054306. doi:10.1103/PhysRevC.82.054306. URL <https://link.aps.org/doi/10.1103/PhysRevC.82.054306>
- S. J. Waldecker, C. Barbieri, W. H. Dickhoff, Microscopic self-energy calculations and dispersive optical-model potentials, *Phys. Rev. C* 84 (2011) 034616. doi:10.1103/PhysRevC.84.034616.

- URL <https://link.aps.org/doi/10.1103/PhysRevC.84.034616>
18. M. H. Mahzoon, R. J. Charity, W. H. Dickhoff, H. Dussan, S. J. Waldecker, Forging the link between nuclear reactions and nuclear structure, *Phys. Rev. Lett.* 112 (2014) 162503. doi:10.1103/PhysRevLett.112.162503. URL <https://link.aps.org/doi/10.1103/PhysRevLett.112.162503>
 19. D. R. Entem, R. Machleidt, Accurate charge-dependent nucleon-nucleon potential at fourth order of chiral perturbation theory, *Phys. Rev. C* 68 (2003) 041001. doi:10.1103/PhysRevC.68.041001. URL <http://link.aps.org/doi/10.1103/PhysRevC.68.041001>
 20. R. B. Wiringa, V. G. J. Stoks, R. Schiavilla, Accurate nucleon-nucleon potential with charge-independence breaking, *Phys. Rev. C* 51 (1) (1995) 38–51. URL <http://link.aps.org/doi/10.1103/PhysRevC.51.38>
 21. L. Ray, G. W. Hoffmann, W. R. Coker, Nonrelativistic and relativistic descriptions of proton-nucleus scattering, *Physics Reports* 212 (1992) 223. doi:https://doi.org/10.1016/0370-1573(92)90156-T. URL <http://www.sciencedirect.com/science/article/pii/037015739290156T>
 22. H. F. Arellano, F. A. Brieva, W. G. Love, In-medium full-folding optical model for nucleon-nucleus elastic scattering, *Phys. Rev. C* 52 (1995) 301–315. doi:10.1103/PhysRevC.52.301. URL <https://link.aps.org/doi/10.1103/PhysRevC.52.301>
 23. H. F. Arellano, E. Bauge, Functional medium dependence of the nonrelativistic optical model potential, *Phys. Rev. C* 76 (2007) 014613. doi:10.1103/PhysRevC.76.014613.
 24. F. J. Aguayo, H. F. Arellano, Surface-peaked medium effects in the interaction of nucleons with finite nuclei, *Phys. Rev. C* 78 (2008) 014608. doi:10.1103/PhysRevC.78.014608.
 25. H. F. Arellano, H. V. von Geramb, Extension of the full-folding optical model for nucleon-nucleus scattering with applications up to 1.5 GeV, *Phys. Rev. C* 66 (2002) 024602. doi:10.1103/PhysRevC.66.024602. URL <https://link.aps.org/doi/10.1103/PhysRevC.66.024602>
 26. J. Dechargé, D. Gogny, Hartree-Fock-Bogolyubov calculations with the $D1$ effective interaction on spherical nuclei, *Phys. Rev. C* 21 (1980) 1568–1593. doi:10.1103/PhysRevC.21.1568. URL <https://link.aps.org/doi/10.1103/PhysRevC.21.1568>
 27. H. F. Arellano, J.-P. Delaroche, Low-density homogeneous symmetric nuclear matter: Disclosing dinucleons in coexisting phases, *Eur. Phys. Journal A* 51 (1) (2015) 7. doi:10.1140/epja/i2015-15007-2. URL <http://link.springer.com/10.1140/epja/i2015-15007-2>
 28. H. F. Arellano, F. Isaule, A. Rios, Di-nucleon structures in homogeneous nuclear matter based on two- and three-nucleon interactions, *Eur. Phys. Journal A* 52 (9) (2016) 299. doi:https://doi.org/10.1140/epja/i2016-16299-2. URL <https://doi.org/10.1140/epja/i2016-16299-2>
 29. F. Isaule, H. F. Arellano, A. Rios, Di-neutrons in neutron matter within a Brueckner-Hartree-Fock approach, *Phys. Rev. C* 94 (2016) 034004. doi:https://doi.org/10.1103/PhysRevC.94.034004. URL <https://link.aps.org/doi/10.1103/PhysRevC.94.034004>
 30. H. F. Arellano, G. Blanchon, SWANLOP: Scattering waves off nonlocal optical potentials in the presence of Coulomb interactions, *Computer Physics Communications* 259 (2021) 107543. doi:https://doi.org/10.1016/j.cpc.2020.107543. URL <http://www.sciencedirect.com/science/article/pii/S0010465520302599>
 31. G. Blanchon, M. Dupuis, H. F. Arellano, R. N. Bernard, B. Morillon, SIDES: Nucleon-nucleus elastic scattering code for nonlocal potential, *Computer Physics Communications* 254 (2020) 107340. doi:https://doi.org/10.1016/j.cpc.2020.107340. URL <http://www.sciencedirect.com/science/article/pii/S0010465520301478>
 32. B. Ridley, J. Turner, Optical model studies of proton scattering at 30 MeV: (I). Differential cross sections for elastic scattering of protons at 30.3 MeV, *Nuclear Physics* 58 (1964) 497 – 508. doi:https://doi.org/10.1016/0029-5582(64)90561-9. URL <http://www.sciencedirect.com/science/article/pii/0029558264905619>
 33. M. P. Fricke, E. E. Gross, B. J. Morton, A. Zucker, Polarization and Differential Cross Section for Elastic Scattering of 40-MeV Protons. II, *Phys. Rev.* 156 (1967) 1207–1218. doi:10.1103/PhysRev.156.1207. URL <https://link.aps.org/doi/10.1103/PhysRev.156.1207>
 34. C. B. Fulmer, J. B. Ball, A. Scott, M. L. Whiten, Elastic Scattering of 61.4-MeV Protons, *Phys. Rev.* 181 (1969) 1565–1579. doi:10.1103/PhysRev.181.1565. URL <https://link.aps.org/doi/10.1103/PhysRev.181.1565>
 35. A. Nadasen, P. Schwandt, P. P. Singh, W. W. Jacobs, A. D. Bacher, P. T. Debevec, M. D. Kaitchuck, J. T. Meek, Elastic scattering of 80-180 mev protons and the proton-nucleus optical potential, *Phys. Rev. C* 23 (1981) 1023–1043. doi:10.1103/PhysRevC.23.1023. URL <https://link.aps.org/doi/10.1103/PhysRevC.23.1023>
 36. D. Hutcheon, W. Olsen, H. Sherif, R. Dymarz, J. Cameron, J. Johansson, P. Kitching, P. Liljestrang, W. McDonald, C. Miller, G. Neilson, D. Sheppard, D. McDaniels, J. Tinsley, P. Schwandt, L. Swenson, C. Stronach, The elastic scattering of intermediate energy protons from 40Ca and 208Pb, *Nuclear Physics A* 483 (3) (1988) 429–460. doi:https://doi.org/10.1016/0375-9474(88)90078-4. URL <https://www.sciencedirect.com/science/article/pii/0375947488900784>
 37. M. Burrows, C. Elster, G. Popa, K. D. Launey, A. Nogga, P. Maris, Ab initio translationally invariant nonlocal one-body densities from no-core shell-model theory, *Phys. Rev. C* 97 (2018) 024325. doi:10.1103/PhysRevC.97.024325. URL <https://link.aps.org/doi/10.1103/PhysRevC.97.024325>
 38. X. Campi, A. Bouyssy, A simple approximation for the nuclear density matrix, *Physics Letters B* 73 (3) (1978) 263–266. doi:https://doi.org/10.1016/0370-2693(78)90509-9.

- URL <https://www.sciencedirect.com/science/article/pii/0370269378905099>
39. H. F. Arellano, F. A. Brieva, W. G. Love, Role of nuclear densities in nucleon elastic scattering, *Phys. Rev. C* 42 (1990) 652–658. doi:10.1103/PhysRevC.42.652.
URL <https://link.aps.org/doi/10.1103/PhysRevC.42.652>
40. G. Bertsch, J. Borysowicz, H. McManus, W. G. Love, Interactions for inelastic scattering derived from realistic potentials, *Nuclear Physics A* 284 (1977) 399–419. doi:10.1016/0375-9474(77)90392-X.
URL <https://www.sciencedirect.com/science/article/pii/037594747790392X>